Solution Structure of Oxidized *Saccharomyces cerevisiae* Iso-1-cytochrome *c*[†,‡]

Lucia Banci,[§] Ivano Bertini,*[,§] Kara L. Bren,[||] Harry B. Gray,[||] Pornthep Sompornpisut,[§] and Paola Turano[§]

Department of Chemistry, University of Florence, Via Gino Capponi 7, 50121 Florence, Italy, and Arthur Amos Noyes Laboratory, California Institute of Technology, Pasadena, California 91125

Received December 10, 1996; Revised Manuscript Received February 3, 1997[⊗]

ABSTRACT: The solution structure of oxidized *Saccharomyces cerevisiae* Cys102Ser iso-1-cytochrome *c* has been determined using 1361 meaningful NOEs (of 1676 total) after extending the published proton assignment [Gao, Y., et al. (1990) *Biochemistry 29*, 6994−7003] to 77% of all proton resonances. The NOE patterns indicate that secondary structure elements are maintained upon oxidation in solution with respect to the solid state and solution structures of the reduced species. Constraints derived from the pseudocontact shifts [diamagnetic reference shift values are those of the reduced protein [Baistrocchi, P., et al. (1996) *Biochemistry 35*, 13788−13796]] were used in the final stages of structure calculations. After restrained energy minimization with constraints from NOEs and pseudocontact shifts, a family of 20 structures with rmsd values of 0.58 ± 0.08 and 1.05 ± 0.10 Å (relative to the average structure) for the backbone and all heavy atoms, respectively, was obtained. The solution structure is compared with the crystal structure and the structures of related systems. Twenty-six amide protons were detected in the NMR spectrum 6 days after the oxidized lyophilized protein was dissolved in D_2O (pH 7.0 and 303 K); in an analogous experiment, 47 protons were observed in the spectrum of the reduced protein. The decrease in the number of nonexchanging amide protons, which mainly are found in the loop regions 14−26 and 75−82, confirms the greater flexibility of the structure of oxidized cytochrome *c* in solution. Our finding of increased solvent accessibility in these loop regions is consistent with proposals that an early step in unfolding the oxidized protein is the opening of the 70−85 loop coupled with dissociation of the Met80−iron bond.

Analysis of the NMR spectra of a protein in solution produces an average structure which may contain information on backbone and side chain fluctuations. Further information on protein structural fluctuations can be obtained through relaxation studies that require stable isotopic labeling (Wagner et al., 1993; Lefevre & Jardetzky, 1994). With unlabeled proteins, the observation of signals due to protons which can be exchanged with solvent and the analysis of the shifts may be informative. In particular, flexibility can be identified by analyzing which amide protons exchange with bulk water. This kind of analysis is most informative when used to compare similar proteins, or different states of one protein (Blanchard et al., 1996).

We are investigating the solution structures of oxidized and reduced forms of *Saccharomyces cerevisiae* iso-1-cytochrome *c*. In particular, we are interested in elucidating those aspects of the protein structure that are related to striking differences in the folding energetics of the two redox states (Bixler et al., 1992; Hilgen-Willis et al., 1993; Cohen & Pielak, 1995; Doyle et al., 1996; Pascher et al., 1996; Mines et al., 1996). It is difficult to understand the magnitude of this difference, $\Delta\Delta G_f \approx 34$ kJ/mol (pH 7, 22.5 °C) (Mines et al., 1996), from crystal structure analyses of the folded proteins; indeed, the structures of the oxidized and reduced forms of the protein in crystals are essentially superimposable (rmsd values of 0.28 Å for the backbone and 0.70 Å for all the heavy atoms) (Berghuis & Brayer, 1992) except for the distorsion of the heme plane and the location of water molecules around the heme, which apparently changes upon reduction (Berghuis et al., 1994). In our work so far, we have determined the NMR solution structure of the reduced Cys102Ser "wild type" protein (Baistrocchi et al., 1996) as well as that of the oxidized cyanide derivative where the Met80 has been mutated to Ala (Banci et al., 1995, 1996a). In this paper, we turn our attention to the solution structure of the oxidized Cys102Ser protein. This protein is relatively large (108 amino acids), indeed, at the limit for structure determination without isotopic labeling. The labeling cannot be done at present because of the lack of adequate expression systems. The protein is also paramagnetic, and paramagnetism is a further difficulty for the assignment and for the observation of proton−proton dipolar connectivities. It provides, however, further structural constraints through the pseudocontact shifts which we have proposed (Banci et al., 1996a,b) to use in the solution structure determination together with the NOEs. We have found that more backbone amide NHs exchange in the oxidized protein than in the reduced form in regions lacking secondary structure elements. Our work suggests that these regions of the protein will be the first to unfold in reactions with denaturing reagents.

The availability of solution structures of oxidized and reduced *S. cerevisiae* cytochrome *c* will eventually lead to

[†] This work was supported by EC Biotechnology Program BIO2-CT94-2052 (DG 12 SSMA), the Italian CNR, and the United States NSF.

[‡] The coordinates of the 20 structures of the PSEUDO-REM family have been deposited in the Brookhaven Protein Data Bank (1YIC).

* Author to whom correspondence should be addressed: Prof. Ivano Bertini, University of Florence, Via Gino Capponi 7, 50121 Florence, Italy. Phone: +39-55-2757549. Fax: +39-55-2757555. E-mail: bertini@risc1.lrm.fi.cnr.it.

[§] University of Florence.

[||] California Institute of Technology.

[⊗] Abstract published in *Advance ACS Abstracts,* April 1, 1997.

S0006-2960(96)03025-5 CCC: $14.00

the quantitative evaluations of the key electron transfer parameters, most notably the reorganization energy (Casimiro et al., 1993; Winkler & Gray, 1992; Langen et al., 1996; Gray & Winkler, 1996). Recent work has shown that the solution structures of the two redox states of horse heart cytochrome *c* (Qi et al., 1996) are not as similar as those we have found for the yeast protein, raising the possibility that the reorganization energy may be larger in the former system. This would be difficult to reconcile with extensive electron transfer kinetics experiments on the horse and yeast proteins, however (Casimiro et al., 1993; Winkler & Gray, 1992; Langen et al., 1996; Gray & Winkler, 1996). Time will tell whether both sets of structures are correct. In the meantime, we report here the full details of our analysis of the solution structure of the oxidized yeast protein.

EXPERIMENTAL PROCEDURES

NMR Sample Preparation. S. cerevisiae iso-1-cytochrome *c* with serine at position 102 (Cys102Ser) was expressed and purified as previously reported (Lu et al., 1993). The ^{1}H NMR samples were prepared by dissolving the lyophilized protein in 50 mM phosphate buffer at pH 7.0 to give 2 mM solutions. The pH of protein samples prepared for NMR spectroscopy was adjusted by addition of small volumes of concentrated solutions of NaOH and H_3PO_4. The pH was measured with an Orion model 720 pH meter and a Microelectrodes, Inc., model MI-410 microcombination pH probe.

NMR Spectroscopy. The ^{1}H NMR spectra were recorded on Bruker MSL 200 and AMX 600 spectrometers operating at 200.13 and 600.13 MHz, respectively. The 200 MHz ^{1}H NMR one-dimensional spectra were recorded using the superWEFT (water-eliminated Fourier transform) (Inubushi & Becker, 1983) pulse sequence with a recycle delay ranging from 200 to 20 ms. The 600 MHz ^{1}H NMR one-dimensional spectra were obtained by using presaturation during the relaxation delay (550−800 ms) or by using a WATERGATE (Piotto et al., 1992; Sklenar et al., 1993) pulse sequence for water signal suppression.

The ^{1}H nuclear Overhauser effect (NOE) experiments (at 200 MHz) were performed with the superWEFT pulse sequence and the data collected using standard methodology (Banci et al., 1989).

TPPI NOESY (Macura et al., 1982; Marion & Wüthrich, 1983) maps at 295 and 303 K in D_2O or H_2O solution were recorded over the full spectral width with a recycle time of 500 ms and a mixing time of 20 ms. To optimize the observation of connectivities in the diamagnetic region, NOESY maps in D_2O and H_2O solutions were recorded on a smaller spectral width (45 ppm), with recycle times of 800 ms and mixing times of 100 ms. Analogously, TPPI HOHAHA (Bax & Davis, 1985) experiments, with presaturation during the relaxation delay, were recorded over a spectral width of 45 ppm (recycle time of 800 ms and spin lock times of 30 and 90 ms). A magnitude COSY (Bax et al., 1981; Bax & Freeman, 1981) map was recorded in H_2O solution over a 45 ppm spectral width (recycle time of 800 ms).

All two-dimensional spectra consisted of 4K data points in the F_2 dimension. From 800 to 1024 experiments were recorded in the F_1 dimension, using 64−192 scans per experiment. Raw data were multiplied in both dimensions by a pure cosine-squared (NOESY and TOCSY) and a pure sine-squared (COSY) bell window function and Fourier-transformed to obtain 2048 × 2048 real data points. A polynomial baseline correction was applied in both directions.

Data processing was performed using a standard Bruker software package. The two-dimensional maps were analyzed on IBM RISC 6000 computers using the aid of the program XEASY (ETH, Zürich) (Eccles et al., 1991).

Proton−Proton Distance Constraints and Structure Calculations. The volumes of the NOESY cross-peaks between assigned resonances were obtained by manual integration (with elliptical integration) using the integration routines present in the program XEASY. Most of the dipolar connectivities were taken from the 100 ms NOESY WATERGATE sequence in H_2O solution at 300 K. Connectivities whose volumes could be better measured in other spectra recorded with the same parameters, but either at a different temperature or in D_2O solution, were scaled referring to a few cross-peaks whose volumes could be accurately measured in both spectra.

NOESY cross-peak intensities were converted into upper limits of interatomic distances by following the methodology of the program CALIBA (Güntert et al., 1991). The detection of one-dimensional NOEs involving paramagnetic signals (for a total of five NOEs) was taken into account in the structure calculations by applying upper distance limits of 4.0 Å when single protons were involved or 6.0 Å for methyl signals.

The experimental distance constraints were then used to generate protein conformers using the distance geometry program DIANA. Upper and lower distance limits were imposed to build up the heme as previously reported (Banci et al., 1995).

DIANA calculations, including the use of the redundant angle strategy routine (REDAC) (Güntert & Wüthrich, 1991), were performed. Initially, 500 random structures were calculated. The final distance geometry calculation on 48 structures was performed without angle constraints to prove convergence. Stereospecific assignments of diastereotopic protons and methyl groups were obtained using the program GLOMSA (Güntert et al., 1991).

Pseudocontact Shift Constraints. The hyperfine shift, i.e., the difference in shift of a proton in the paramagnetic system from that in an analogous diamagnetic system, includes contact and pseudocontact contributions (La Mar et al., 1973; Bertini & Luchinat, 1986, 1996; Bertini & Turano, 1994). The contact coupling is due to the presence of unpaired spin density on the resonating nucleus and vanishes a few chemical bonds away from the metal. The pseudocontact contribution (δ_{pc}) arises from the magnetic susceptibility anisotropy and depends on the nuclear position with respect to the principal axes of the magnetic susceptibility tensor:

$$\delta_{pc} = \frac{1}{12\pi r^3}[\Delta\chi_{ax}(3n_i^2 - 1) + 3/2\Delta\chi_{rh}(l_i^2 - m_i^2)] \quad (1)$$

where $\Delta\chi_{ax}$ and $\Delta\chi_{rh}$ are the axial and the rhombic anisotropy of the magnetic susceptibility induced by the paramagnetic ion, respectively, r_i is the distance of the nucleus i from the ion, and l_i, m_i, and n_i are the direction cosines of the position vector of atom i ($\mathbf{r}_i$) with respect to the orthogonal reference system formed by the principal axes of the magnetic susceptibility tensor.

If a single structure is available, the five independent parameters (i.e., $\Delta\chi_{ax}$, $\Delta\chi_{rh}$, and three independent direction

cosines which define the principal directions of the tensor with respect to a metal-centered axis system) can be determined by finding the best fit of eq 1 to a set of pseudocontact shifts. For a family of N structures, an average magnetic susceptibility tensor can be determined by fitting an extended set of equations (eq 1) with N slightly different $\mathbf{r}_i$ vectors to the same set of experimental pseudocontact shift values. This calculation was performed by the program FANTASIA (Banci et al., 1996a).

The magnetic susceptibility tensor parameters derived from these calculations were then used in a modified version of the DIANA program, called PSEUDIANA (Banci et al., 1996a), to introduce the pseudocontact shifts as further constraints for the structure calculation, as reported for the Met80Ala cytochrome *c* mutant (Banci et al., 1996a). In these calculations, the pseudocontact shifts were weighted as much as the NOEs.

Finally, restrained energy minimization (REM) with the Sander module of Amber (Pearlman & Case, 1991) was applied to 48 structures. Pseudocontact shifts were included as constraints in a modified Sander module (Banci et al., 1996b).

Structure calculations and analysis were performed on an IBM SP02 parallel computer.

RESULTS AND DISCUSSION

Sequence-Specific Assignment. An extensive sequence-specific assignment of the protein residue resonances in the ^{1}H NMR spectrum of oxidized (Cys102Thr) *S. cerevisiae* iso-1-cytochrome *c* (cyt *c* hereafter) at 300 K (pH and buffer were not reported) is available (Gao et al., 1990). We have repeated the assignment of the protein residues for oxidized (Cys102Ser) *S. cerevisiae* iso-1-cytochrome *c* under our experimental conditions (50 mM phosphate buffer at pH 7.0), and we also have assigned all the heme resonances (only a partial assignment was done previously).

The protein residues have been assigned through analysis of TOCSY and COSY maps in H_2O and D_2O for the location of spin patterns and NOESY maps in H_2O for identification of sequential NH−NH and Hα−NH connectivities. Assignment of the hyperfine-shifted signals of the heme, its axial ligands, and the heme-bound Cys14 and Cys17 was done through NOESY experiments tailored to the relaxation properties of these paramagnetic resonances and through one-dimensional NOE experiments.

The two first residues at the N terminus and Gly83 remain unidentified. Assignments of most of the resonances are consistent with those already reported (Gao et al., 1990). Newly assigned resonances are given in Table 1. In total, 77% of the expected proton resonances have been assigned.

Secondary Structure. Figure 1 shows the short- and medium-range NOEs, observed for the backbone protons in the 100 ms NOESY map in water. Sequential NH−NH connectivities for stretches longer than two amino acids have been observed for residues 2−5, 6−15, 16−18, 31−33, 36−38, 41−43, 50−55, 61−70, 72−75, 79−82, 89−92, and 93−103. Four prolines are present in the sequence, which break the sequential NH−NH connectivities. Moreover, the amide resonances of five residues, in addition to the two N-terminal unassigned amino acids (−4, 26, 45, and 47), have not been located.

Helical structures, characterized by strong NH−NH and medium-range Hα−NH(i,i+3), Hα−Hβ(i,i+3), and Hα−NH(i,i+4) NOEs, are present in segments 6−13, 50−55, 61−69, 70−75, and 89−103 (Figure 1); Hα−NH(i,i+2) NOEs, indicative of a 3_{10}-helical conformation (Wüthrich, 1986), are seen in segments 6−12, 62−69, and 70-75. Moreover, (i,i+3) and (i,i+2) connectivities also have been observed for residues 14−18, thus suggesting some type of helical structure (Detlefsen et al., 1991; Marion & Guerlesquin, 1992; Blackledge et al., 1995; Baistrocchi et al., 1996; Banci et al., 1995). All of these secondary structure

Table 1: New Proton Assignments Obtained in the Present Work for the Oxidized *S. cerevisiae* Iso-1-cytochrome *c*[a]

residue	HN	α	β	others
Lys2				δ 1.48, 1.52; ε 2.85
Lys5				γ 0.86
Phe10				δ 7.20; ε 7.79[b]
Lys11			1.82, 2.18[c]	γ 1.48
Arg13			1.00, 1.38[d]	γ 1.24, 1.65
Cys14		1.45	2.66, 2.94	
Leu15				δCH$_3$ 1.46, 2.04[e]
Gln16				γ 2.85, 3.00[f]; ε 6.86, 7.56
Cys17			3.03[g], 2.46	
Pro25				γ 2.56; δ 3.64
Leu32				δCH$_3$ 0.90, 1.43
Arg38			1.82	γ 1.97; δ 3.24[h]
His39				δCH 6.66; εCH 7.84[i]
Ser40			3.62, 4.15[j]	
Gly45		3.72, 4.29		
Tyr46				δ 4.65, 5.74; ε 3.67, 5.06[k]
Lys54			1.60, 1.86	
Lys55			1.97, 2.06[l]	γ 1.38
Glu61				γ 0.87
Met64			2.19, 2.38	γ 1.74[m]
Glu66				γ 2.25, 2.44
Tyr67				δ 7.51; ε 7.77
Pro71		5.69	5.03, 5.65	γ 2.26, 4.54; δ 2.83, 3.90[n]
Tml72				γ 1.37, 2.38; ε 3.98;
Lys73				γ 1.71; δ 1.93; ε 3.21
Tyr74		4.76[o]		
Thr78				OH 9.71
Lys79			1.38, 1.72	γ 0.16, 1.03; δ 0.70; ε 2.09, 2.33
Met80	8.86[p]			
Phe82			2.76, 3.09	
Lys86				γ 1.42
Asp93			2.45, 2.65[q]	
Ile95				γ 0.32, 1.39; γCH$_3$ 0.24[r]
Lys99				γ 0.65; δ 0.80
Ser102	7.67		3.24	

Heme Assignments

α-meso 2.66, β-meso 1.71, γ-meso 8.03,[s] δ-meso 2.34, 6-Hα 2.88, 6-Hα′ −1.43, 6-Hβ 1.03, 6-Hβ′ 2.66, 7-Hα 12.72, 7-Hα′ 15.91, 7-Hβ 1.34, 7-Hβ′ −0.23

[a] The shift values are measured at 303 K. The assignments of the other resonances were reported previously by Gao et al. (1990). [b] δ and ε proton assignment is reversed with respect to the previous work. [c] Only one of the two β protons was previously assigned (at 2.18 ppm). [d] Only one of the two β protons was previously assigned (at 1.00 ppm). [e] Only one of the two δ CH$_3$ resonances was previously assigned (at 1.48 ppm). [f] Only one of the two γ protons was previously assigned (at 2.98 ppm). [g] The assignment for this proton was different in the previous work. [h] The assignment of the side chain resonances for this residue was different (and more extensive). [i] The assignment of the ring proton resonances for this residue was different. [j] Only one of the two β protons was previously assigned (at 3.62 ppm). [k] δ and ε proton assignment was partially different in the previous work. [l] Only one of the two β protons was previously assigned (at 1.94 ppm). [m] The assignment of the side chain resonances for this residue was different (and more extensive). [n] The assignment of the side chain resonances for this residue was different. [o] This resonance was previously assigned at 5.18 ppm. [p] Previously assigned at 9.70 ppm (where we have now assigned the OH of Thr78). [q] Only one of the two β protons was previously assigned (at 2.47 ppm). [r] The assignment of the γ CH$_3$ group has been modified. [s] The assignment of this proton was different in the previous work.

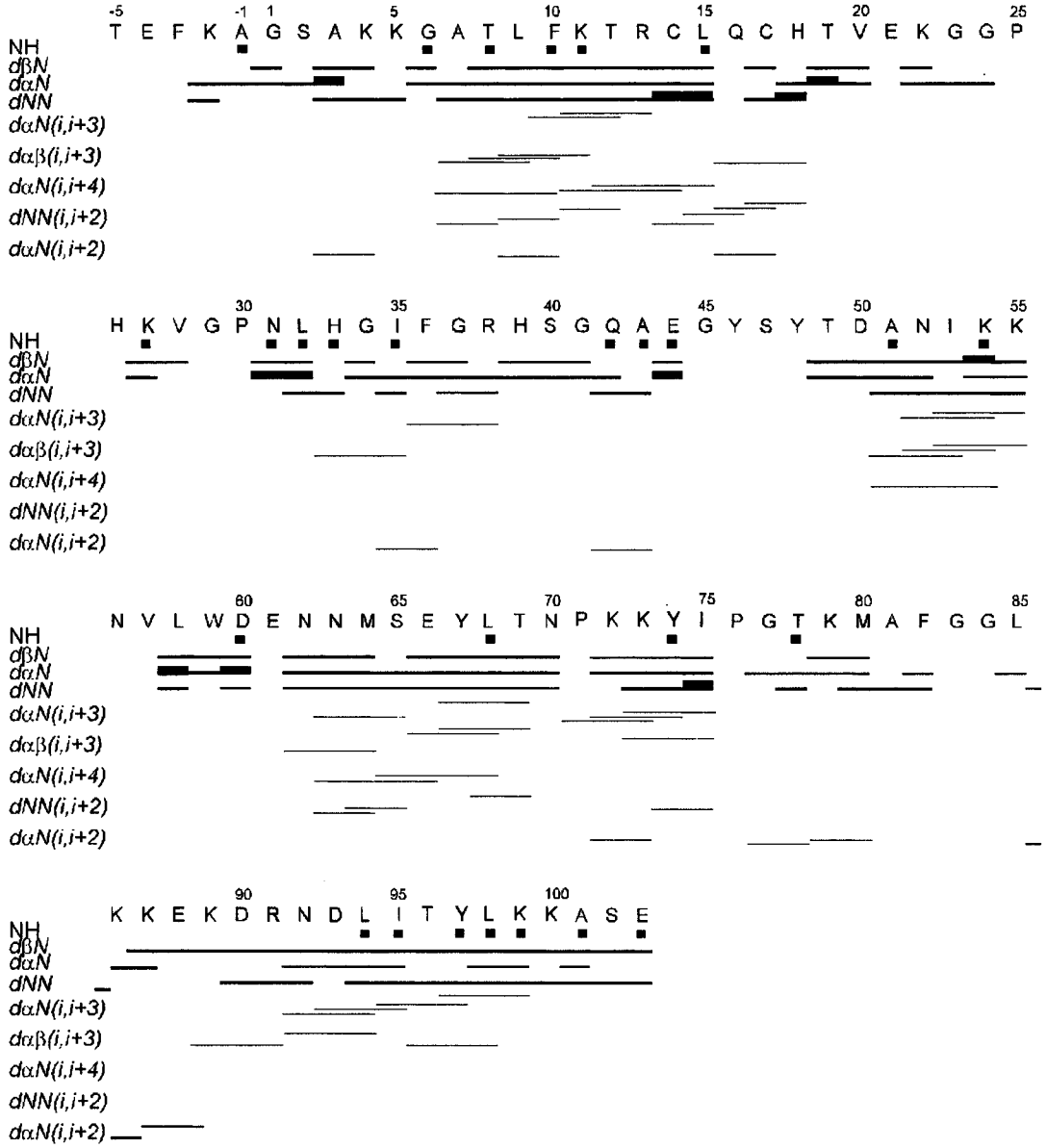

FIGURE 1: Sequential dipolar connectivities involving NH, Hα, and Hβ protons in oxidized *S. cerevisiae* iso-1-cytochrome *c*. The thickness of each bar indicates the relative NOE intensity. In the first line, NH resonances associated with protons that exchange slowly in D_2O solution are indicated by filled squares.

elements are similar to those present in the solution structure of reduced cyt *c* (Baistrocchi et al., 1996).

Solution Structure Calculations. Experimental NOESY constraints (1671) were assigned and integrated. These NOE constraints were transformed into upper distance limits with the program CALIBA (Güntert et al., 1991), which uses a volume-to-distance correlation. The best calibration of observed intensities was found to be inversely proportional to the fifth or sixth power of the proton−proton distances, depending on the calibration class of NOE constraints.

A total of 1361 out of 1676 experimental constraints were found to be meaningful and therefore taken into account by the program DIANA (Güntert et al., 1991) during the distance geometry calculations. The number of experimental NOE constraints per residue is shown in Figure 2. It corresponds to 15.5 experimental NOEs per residue as input and to 12.6 accepted NOEs per residue.

The heme group, the axial ligands, and the two Cys residues covalently linked to the porphyrin were treated as before (Banci et al., 1995). Five hundred structures were initially calculated. Forty-two stereospecific assignments of the diastereotopic protons were obtained with the program GLOMSA (Güntert et al., 1991); 14 hydrogen bond constraints, involving slowly exchanging amide protons consistently present in the initially calculated DG structures, were introduced as further constraints in the final stages of the structure calculations.

The DG family (DG1) obtained using the constraints from NOE connectivities and hydrogen bonds consists of the 20 structures with the lowest target function (i.e., $\leq$1.16 Å^2) and with individual violations not exceeding 0.35 Å. The target function (TF) is a measure of the discrepancy between the experimental and calculated NOE constraints:

$$\mathrm{TF} = \sum_{c=u,l,v} w_c \sum_{i \in I_c} \left\langle \Theta_c \left\langle \frac{d_i^{c2} - b_i^{c2}}{2 b_i^{c}} \right\rangle \right\rangle^2 + w_a \sum_{i=1}^{n_a} \left\langle 1 - {}^1\!/_2 \left\langle \frac{\Delta_i}{\Gamma_i} \right\rangle^2 \right\rangle \Delta_i^2 \quad (2)$$

with

$$\Theta_c(t) = \begin{cases} \max(0, t) & \text{if } c = \mu \\ \min(0, t) & \text{if } c = l, \nu \end{cases}$$

and d_i^c and b_i^c are the calculated and observed distances between two atoms in the structure, respectively, and w_c (>0) is the weighting factor for the four types of constraints ($c = u$, l, v, and a; u = upper limits, l = lower limits, v = van der Waals repulsion lower limits on interatomic distances and a dihedral angle constraints) (Güntert et al., 1991).

The rmsd values for the DG1 family with respect to the mean structure are 0.63 ± 0.06 Å for the backbone atoms and 1.10 ± 0.08 Å for all heavy atoms (Table 2).

During the final stages of the structure calculations, pseudocontact shifts also were included as constraints. This procedure, which already has been used for refinement of solution structures of paramagnetic metalloproteins (Banci et al., 1996a), turned out to be quite efficient. The pseudocontact shifts are long-range constraints, since they depend on the inverse of the third power of the metal−proton distance, while the NOEs depend on the inverse of the sixth power of the proton−proton distance. Furthermore, they connect the metal ion with protons. The pseudocontact shifts are a function of the coordinates of the nuclei relative to the molecular axis system centered on the metal ion. Therefore, they can be used as constraints (both angular and radial) for structure determination if the anisotropy and the principal directions of the magnetic susceptibility tensor are known. This requirement can be met if a reasonable starting structure is available for the system under study. Indeed, it has been shown that pseudocontact shift constraints can be used to refine X-ray crystal structures (Gochin & Roder, 1995).

We developed this approach to refine NMR solution structures. Both NOEs and pseudocontact shifts are used to recalculate the structure through the PSEUDIANA program (Banci et al., 1996a). A new family of structures is obtained for which a new magnetic susceptibility tensor could be calculated. The entire procedure is repeated until self-consistency is achieved, i.e., until the parameters do not vary by more than 1%. After that, restrained energy minimization calculations with the PSEUDO-REM (Banci et al., 1996b) program, which includes both NOE and pseudocontact shift constraints, can be performed.

In the present paper, the pseudocontact contribution to the shift for oxidized cyt *c* has been evaluated for protons of residues not directly bound to the heme by subtracting the shift observed for the same proton in the reduced protein (Baistrocchi et al., 1996). For diastereotopic protons, only those stereospecifically assigned in both oxidation states have been taken into account. In Figure 3, the distribution of the pseudocontact shifts (δ_{pc}) for the various residues is reported. The protons either with large δ_{pc} ($\delta_{pc} > 1$ ppm) or with any pseudocontact shift but located within a 10 Å sphere centered on iron are reported in Table 3, together with their distance from the iron. Here it is assumed that the pseudocontact shift term is metal-centered. That means that it is assumed that the unpaired electron is located on iron. Of course, this is an approximation which is expected to be good for protons far from the metal ion. We are testing here how pseudocontact shifts can be used within this approximation.

The disagreement between experimental and calculated pseudocontact shifts is contributing to the target function (see earlier) only if the disagreement exceeds a chosen tolerance.

The choice of the tolerance is related to the estimated error in the values of the pseudocontact shifts, and to the error in evaluating the pseudocontact shifts through eq 1, as a result of protein mobility and of the indetermination on the position of the atoms due to the existence of a family rather than a single structure. As the observed shifts can be measured with a high level of precision, the main error in estimating the experimental δ_{pc} values arises from the choice of the diamagnetic reference. In principle, structural differences may be present in the reduced state with respect to the oxidized state that could affect the evaluation of the diamagnetic shifts. This would be particularly meaningful for NH protons. The final choice of the tolerance, therefore, may depend on the system under investigation and on the quality of the structure to be refined. The a posteriori verification of low target functions for NOEs and δ_{pc} is however needed. A value of 0.3 ppm takes into account possible sources of indetermination in the actual pseudocontact shifts versus the calculated ones and leads to an appreciable refinement of the structure.

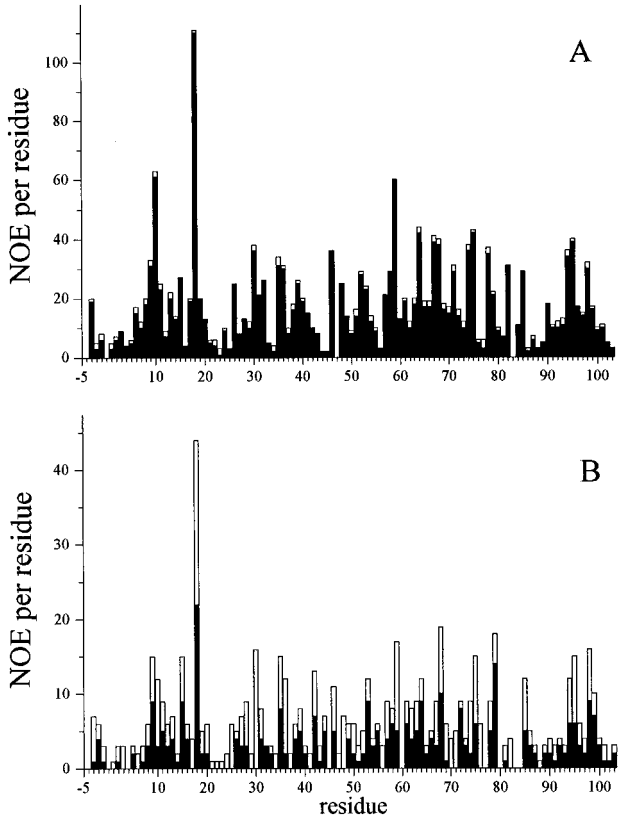

FIGURE 2: Number of inter- (A) and intra (B)-NOEs per residue in the NMR spectra. The total height of each column represents the amount of observed experimental NOEs. The open and filled bars correspond to NOE constraints that are irrelevant and meaningful, respectively.

An average magnetic susceptibility tensor was calculated for the 20 structures in the DG1 family by fitting the experimental δ_{pc} values and using a tolerance of 0.3 ppm. This tensor was then utilized in the following PSEUDIANA calculations on the best 48 structures in terms of target function. The resulting PSEUDO-DG2 family consists of the 20 structures with the lowest total target function (i.e., $\leq$7.12 Å^2) and with a residual NOE violation not exceeding 0.50 Å^2. The rmsd values with respect to the mean structure for this family are 0.58 ± 0.07 and 1.05 ± 0.07 Å for the backbone and all heavy atoms, respectively. Finally, from the best 48 structures of PSEUDIANA calculation, energy minimization with the module called PSEUDO-REM (Banci et al., 1996b) was performed. A family of the best 20

Table 2: rmsd Values with Respect to the Average Structure for the Backbone (BB) and All Heavy Atoms (HA) for the DG1, PSEUDO-DG2, and PSEUDO-REM Families of Structures of *S. cerevisiae* Cytochrome *c*[a]

	DG1	PSEUDO-DG2	PSEUDO-REM
rmsd for residues 1−102 (Å)			
BB	0.63 ± 0.06	0.58 ± 0.07	0.58 ± 0.08
HA	1.10 ± 0.08	1.05 ± 0.07	1.05 ± 0.10
total target function (Å^2)	≤1.16	≤7.12	≤4.10
NOEs' target function (Å^2)	−	≤1.29	≤0.87
δ_{pc} target function (Å^2)	−	≤5.01	≤3.42
total energy (kJ mol^{-1})	−	−	−4556.2
deviation from ideal bond distance (Å)			0.008
deviation from ideal bond angles (deg)			1.84

[a] The 20 structures of each family are those with the lowest target function values among all the calculated structures.

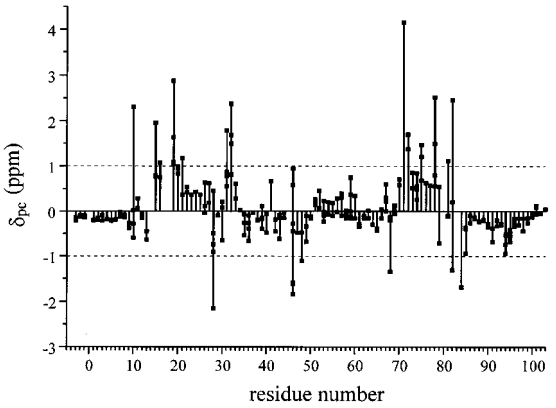

FIGURE 3: Distribution of pseudocontact shifts (δ_{pc}) in the protein residues. The filled squares represent the pseudocontact shift values of the various protons in the given residue.

structures (in terms of target function) with rmsds of 0.58 ± 0.08 and 1.05 ± 0.10 Å and a target function in the 3.58−4.10 Å^2 range is obtained. These values are quite satisfactory, especially if it is considered that the contribution of the NOE is essentially the same (<1.0 Å^2) before and after introducing the pseudocontact shift constraints. This means that the two types of constraints are compatible within the present approach. The overall reduction in the rmsd values upon introduction of the pseudocontact shift constraints mainly reflects the improvement in the positioning of the residues that are closer to the heme iron and are not involved in secondary structure elements (i.e., 15−19 and 76−86). This can be clearly seen from the rmsd comparisons shown in Figure 4.

The rmsd values between the average structures from the DG1 and PSEUDO-REM calculations are 0.75 and 1.03 Å for the backbone and all heavy atoms, respectively. This indicates that the two calculation procedures produce similar results.

The total number of pseudocontact shift values is 256. When all the pseudocontact shift constraints were introduced for the first time in the structure calculations (at the level of PSEUDIANA), 113 resonances had deviations between the calculated and experimental pseudocontact shift values that were larger, in absolute value, than the tolerance, in this case set at 0.3 ppm. At the end of PSEUDO-REM calculation, about 35 resonances had deviations larger than 0.3 ppm (and only six resonances had deviations larger than 0.4 ppm, but not exceeding 0.6 ppm). The violations are mostly due to exchangeable protons, as expected, because the used tolerance could be small with respect to the uncertainty on the shifts of the diamagnetic reference.

This behavior would suggest than an analysis of the pseudocontact shifts with an initial structural model might be unsound because the molecule has not been allowed to reach a structure consistent with the pseudocontact shifts. This presumably is what happened in an early investigation where the pseudocontact shifts were calculated on the basis of the X-ray structure (Gao et al., 1991a,b). However, a few cycles of minimization lead to a structure completely consistent with the experimental pseudocontact shifts. The shift values used are reported as Supporting Information.

The energy-minimized average structure (Figure 5) calculated from the above PSEUDO-REM family of 20 structures has been used to check the quality of the structure by a Ramachandran plot. Among the 90 residues which are "meaningful" for the Ramachandran plot (i.e., non-glycine, non-proline, and nonterminal residues), 62 fall in the most favored regions and 27 in the additional allowed regions. His26 falls in a generously allowed region.

Table 3: Protons Located within a 10 Å Sphere Centered on the Heme Iron and Protons Experiencing Large δ_{pc}'s[a]

residue	proton	δ_{pc} (ppm)	distance (Å)	residue	proton	δ_{pc} (ppm)	distance (Å)
Phe10	Hα	−0.59	9.4	Tyr46	Hβ	−1.58	10.5
	Hζ	2.31	7.9		Hδ	−1.61	8.6
Arg13	Hα	−0.63	9.5	Tyr48	Hα	−1.10	9.9
Leu15	HN	0.77	8.3	Trp59	Hζ	0.37	9.8
	Hα	1.96	8.2		Hζ'	0.00	8.0
Gln16	HN	1.08	8.1		HNϵ	−0.13	8.6
Thr19	HN	2.88	7.6	Tyr67	Hδ	0.31	7.4
	Hα	1.64	9.1		Hδ'	0.31	8.7
	Hβ	1.05	11.1		Hϵ	0.22	5.0
	γCH$_3$	1.10	11.3		Hϵ'	0.22	7.0
Val20	Hα	0.99	9.6	Leu68	HN	−0.20	9.1
	Hβ	0.83	9.3		Hα	−0.13	7.4
Glu21	HN	1.18	11.1		Hγ	−1.34	8.0
His26	Hα	0.64	9.5	Pro71	Hβ	4.15	6.2
Lys27	HN	0.62	9.0	Tml72	HN	1.70	8.8
Val28	HN	0.46	8.1		Hα	1.38	9.3
	Hα	−0.91	9.0	Ile75	HN	1.21	10.6
	Hβ	−0.74	7.1		Hβ	1.48	9.2
	γCH$_3$	−2.15	7.0	Thr78	Hα	0.56	9.0
	γ'CH$_3$	−0.49	9.4		Hβ	1.50	8.2
Gly29	HN	−0.09	6.2		γCH$_3$	2.52	7.7
Pro30	Hα	0.21	8.2	Lys79	HN	−0.71	8.1
	Hβ	0.08	8.2		Hα	0.55	8.9
	H$'\beta$	−0.64	8.5	Ala81	HN	−0.09	6.4
Leu32	HN	1.69	8.0		Hα	1.12	8.2
	Hα	0.82	8.2		βCH$_3$	−0.11	8.9
	δCH$_3$	2.38	5.9	Phe82	HN	2.46	6.3
	δ'CH$_3$	1.50	5.0		Hα	0.21	6.6
Ile35	Hβ	−0.04	9.1		Hζ	−1.30	8.1
				Gly84	HN	−1.68	9.2
				Leu85	HN	−0.36	9.7
					Hγ	−0.94	9.2

[a] $|\delta_{pc}| > 1.0$ ppm. The proton−iron distance is also reported. Distances were calculated from the energy-minimized structure obtained from the best 20 structures calculated by PSEUDO-REM.

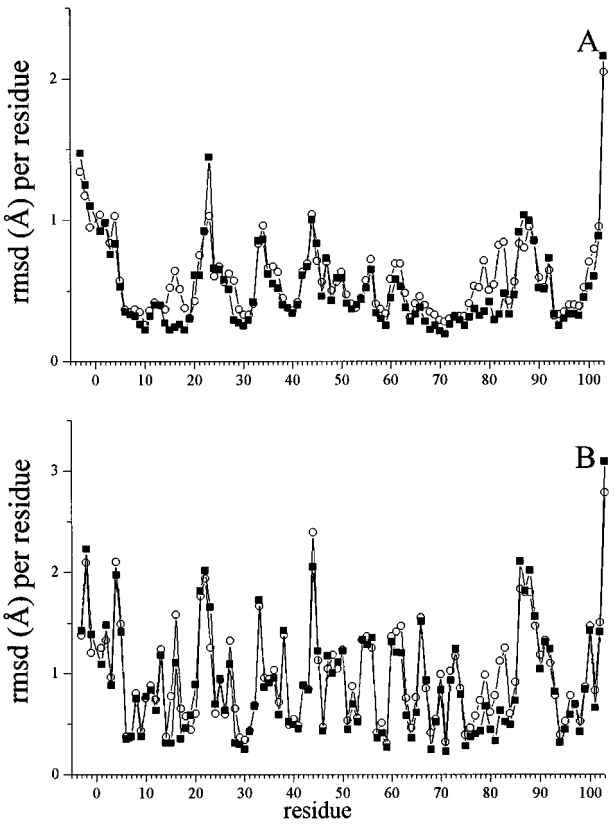

FIGURE 4: Diagrams of the rmsd (with respect to the average structure) per residue for the backbone (A) and all heavy atoms (B) for the 20 structures in the DG1 (○) and PSEUDO-REM (■) families.

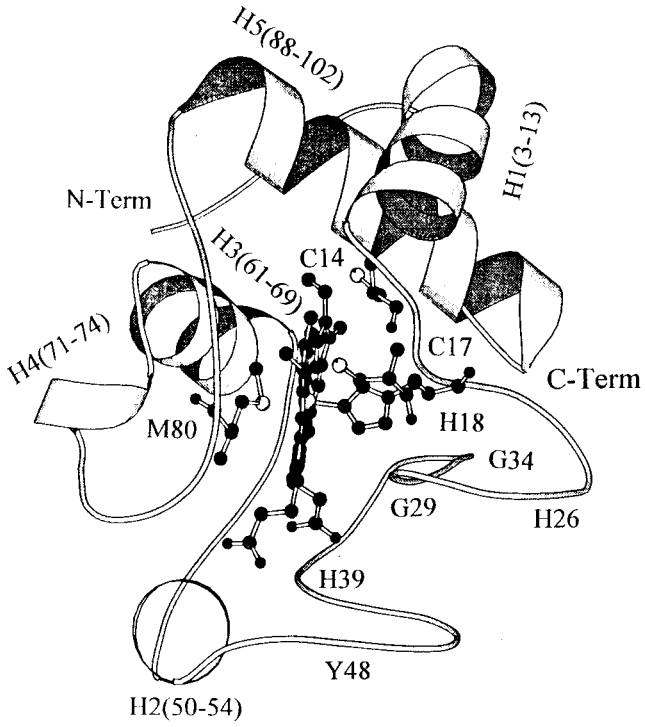

FIGURE 5: Ribbon diagram of the solution structure of oxidized *S. cerevisiae* iso-1-cytochrome *c*, displayed using MOLSCRIPT (Kraulis, 1991). The structure was obtained by energy-minimizing the average of the 20 solution structures in the PSEUDO-REM family. The five helices are denoted H1−H5.

In a recent paper (Qi et al., 1996) on horse heart cyt *c*, the pseudocontact shifts have been used to obtain distance constraints from iron and from the pyrrole nitrogens. Such constraints have then been used together with NOEs within a MD approach. The resulting structure has rmsd with that obtained only from NOEs of ∼1.3 Å for all atoms.

Magnetic Susceptibility Tensor. The magnetic susceptibility tensor parameters obtained from the above-described method should be reliable because they are based on an actual solution structure.

It is interesting to note that, although the $\Delta\chi_{ax}$ and $\Delta\chi_{rh}$ values change slightly from one step to another, the direction of the magnetic axes remains the same. The final tensor has $\Delta\chi_{ax}$ and $\Delta\chi_{rh}$ values of $(2.22 \pm 0.07) \times 10^{-32}$ and $(1.04 \pm 0.07) \times 10^{-32}$ m^3, respectively. The χ_{xx} and χ_{yy} axes are essentially aligned along the pyrrole nitrogen atoms (within 9°), while the χ_{zz} axis deviates by about 17° from the normal to the heme plane. The final tensor obtained from our calculations has an orientation similar to that previously found by using the pseudocontact shift values of *S. cerevisiae* iso-1-cytochrome *c* by assuming that the X-ray crystal structure is the actual solution structure (Gao et al., 1991a). In the latter calculations, it has been found that the rhombic axes deviate by 6° from the line connecting opposite nitrogens of the heme and the angle between the magnetic *z*-axis and the heme normal is 9°. In the case of tuna cyt *c*, the in-plane axes are rotated by 2° with respect to the pyrrole nitrogens, and the *z*-axis makes an angle of 11°, respectively with respect to the heme normal (Williams et al., 1985). In cytochrome *c* from horse heart, these angles are 7° and 14°, respectively (Feng et al., 1990). The evaluation of the magnetic susceptibility anisotropy parameters using either the solution or the crystal structures of horse heart cytochrome *c* gave similar rotation angles (11 and 15°, respectively), while the g_{ax} and g_{rh} values differ significantly (5.15 and −1.65 determined using the crystal structure and 3.43 and −2.55 using the solution structure, respectively) (Qi et al., 1996).[1] In all these cytochromes, the positive *x*-axis is aligned along the pyrrole I nitrogen. It has already been suggested that the tilt of the *z*-axis with respect to the heme normal reflects the tilt of the Fe−S(Met80) bond.

The magnetic susceptibility tensor for oxidized *S. cerevisiae* cyt *c* differs from that for the cyanide adduct of the Met80Ala protein (Banci et al., 1996a); in the latter case, the rhombic axes are approximately aligned along the heme meso carbons and the *z*-axis is orthogonal to the heme plane. Since the Fe−CN unit has cylindrical symmetry, the rhombicity must be attributable to the orientation of the imidazole plane of the proximal ligand (Turner, 1995). In contrast, the sixth ligand in the coordination sphere of oxidized cytochrome *c* is the sulfur of a methionine, whose π interaction with iron contributes significantly to the orientation of the rhombic magnetic axes, in the heme plane and orthogonal to it (Turner, 1995).

Exchange of Amide Protons. NOESY spectra of the oxidized and reduced forms also were recorded at different times (0, 1, 2, and 6 days) after the protein was dissolved in D_2O buffer. The nonexchanging amide protons mainly belong to residues involved in α-helices with the exception of the helices involving residues 61−75. Those exchanging within 6 days in both oxidation states belong to loops.

The number of exchanging amide protons is strikingly different for the reduced and the oxidized forms of yeast

[1] Assuming a temperature of 300 K, these values, expressed as $\Delta\chi$, yield the following results: $\Delta\chi_{ax} = 3.35 \times 10^{-32}$ m^3 and $\Delta\chi_{rh} = -1.1 \times 10^{-32}$ m^3 for the crystal structure and $\Delta\chi_{ax} = 2.23 \times 10^{-32}$ m^3 and $\Delta\chi_{rh} = -1.66 \times 10^{-32}$ m^3 for the solution structure.

cyt *c* at pH 7.0 and 303 K; ^{1}H NMR signals of 47 NH protons are detected in D_2O solutions for the reduced cyt *c* (Baistrocchi et al., 1996), whereas only 26 NH signals are observed for the oxidized protein (Figure 1). A difference, even if smaller, in the number of non-exchanging protons between the oxidized and reduced forms has also been observed at pH 4.6 (Marmorino et al., 1993). The comparison was made under the same experimental conditions a week after sample preparation. The protons experiencing exchange in the oxidized form at variance with the reduced form are mainly located in the protein segments 14−26 and 75−82, i.e., in regions outside the helical structures. There are also a few scattered amide protons which do not exchange in the oxidized form but do in the reduced form of the protein.

Amide protons can exchange with bulk solvent protons or deuterons through fluctuactions which allow the water molecules to reach the exchangeable protons and then to perform the exchange (Hvidt & Nielsen, 1966; Englander & Kallenbach, 1983; Englander, 1992; Bai et al., 1995).

Since oxidized cyt *c* is much more readily unfolded than the reduced protein (Pascher et al., 1996), it is reasonable to assume that exchangeable protons are more accesible to the bulk solvent, and therefore, many more of them will exchange in the oxidized protein.

It has been suggested that amide hydrogen exchange in oxidized cyt *c* is most probable in regions where there are structural fluctuations (Bai et al., 1995). Our work indicates that the flexibility of the structure in the 14−26 and 75−82 regions is greater in the oxidized than in the reduced protein. The first segment, in addition to the covalently attached cysteines and the axial ligand histidine, contains one loop extending toward the exterior of the protein. The second segment contains the Met axial ligand. Interestingly, the lowest energy unfolding step in horse heart cyt *c* appears to be the opening of the 70−85 loop, which is accompanied by disruption of the Met80−Fe bond (Bai et al., 1995; Elove et al., 1994; Doyle et al., 1996). The larger number of exchangeable protons in the oxidized protein may be related to electrostatic effects due to the additional positive charge on the iron center.

In the cyanide adduct of the oxidized Met80Ala mutant, only the NHs of Cys14 and Leu15 in the 14−26 segment and of Ile75 in the 75−82 segment do not exchange in D_2O under the above conditions (Banci et al., 1995). The main difference in the exchange behavior between oxidized cyt *c* and the Met80Ala mutant is observed in the 30−35 segment; in the mutant only, the His33 amide proton does not exchange (Banci et al., 1995), whereas in the oxidized native protein, the following four amide protons of Arg31, Leu32, His33, and Ile35 do not exchange. The 30−35 segment does not show any secondary structure but is in contact with segment 14−25. The following hydrogen bonds involving atoms in these segments are observed in the solution structure of oxidized cyt *c*: Glu21 NH−Asn31 Oδ1 (all calculated structures), Asn31NH−His26 Nδ1 (all calculated structures), and Asn31 H22−Thr19 Oγ1 (50% of calculated structures). Similar, although not identical, hydrogen bond interactions between side chain and main chain atoms in these segments are observed in the solution structure of reduced cyt *c* (Baistrocchi et al., 1996). Interestingly, such interactions are absent in the solution structure of the Met80Ala mutant, and this may account for the larger number of exchangeable protons in this protein segment.

Table 4: rmsd Values for the Backbone (BB) and All Heavy Atoms (HA) of the Energy-Minimized Average Solution Structure (PSEUDO-REM Family) of Oxidized *S. cerevisiae* Iso-1-cytochrome *c*[a]

	⟨red cyt c⟩	⟨Met80Ala⟩	X-ox	X-red	cyt c:CcP
BB	0.97	1.01	0.88	0.86	0.80
HA	1.72	1.70	1.56	1.52	2.25

[a] Values are relative to (i) energy-minimized average solution structures of reduced cyt *c* (⟨red cyt c⟩) (Baistrocchi et al., 1996), (ii) the energy-minimized oxidized cyanide adduct of Met80Ala cyt *c* (⟨Met80Ala⟩) (Banci et al., 1995), crystal structures of (iii) oxidized (Berghuis & Brayer, 1992) and (iv) reduced (Louie & Brayer, 1990) *S. cerevisiae* cytochrome *c* (X-ox and X-red, respectively), and (v) the structure of the oxidized cytochrome *c*−cytochrome *c* peroxidase complex (cyt c:CcP) (Pelletier & Kraut, 1992).

Structural Comparisons. Five structures for wild type *S. cerevisiae* iso-1-cytochrome *c* are now available; these are the solution structures of the reduced (Baistrocchi et al., 1996) and oxidized proteins, the X-ray crystal structures of the reduced (Louie & Brayer, 1990) and oxidized (Berghuis & Brayer, 1992) uncomplexed species, and the X-ray crystal structure of the oxidized protein in the cyt *c*−CcP complex (Pelletier & Kraut, 1992). We have compared the present solution structure with all the others (Table 4).

Comparisons of the structures of the oxidized and reduced forms of cytochrome *c* are important as the atomic displacements contribute to the electron transfer reorganization energy (Scott, 1996). Much attention has been directed to comparisons of X-ray structures of crystals of *S. cerevisiae* cytochrome *c* in the same space group (i.e., $P4_32_12$), which show that the heme distortion is more severe in the oxidized state (Mer et al., 1994). Comparison has been performed also between the X-ray structures of tuna cytochrome *c* in the two oxidation states, which has led to observations similar to those for *S. cerevisiae* cyt *c* (Takano & Dickerson, 1981a,b). With the present experimental data in hand, however, we cannot tell whether the difference in heme structure is present in solution. In the crystal, a rearrangement of propionate 7 occurs upon oxidation that allows this group to form an H bond with the NH of Gly41. We also see this rearrangement in our solution structures. In the solid state, the angle made by the His18 imidazole with the heme pyrrole nitrogens differs by 8° between the two oxidation states. This angle is within the error limits of our solution structures. The X-ray structures show that, upon oxidation, an H bond is formed between the NH of Arg13 and the CO of Gly84, whereas in solution, Arg13 has a different orientation so that no H bond is formed between the two residues in either oxidation state. The mobility of the loops connecting the α-helices has been discussed in the previous section. Concerning dynamical properties, it is of interest that the aromatic ring of Tyr67 has a different mobility in the solution structures of the reduced and oxidized proteins. Indeed, in the reduced form, four signals are detected for the aromatic protons which indicate that the flipping of the aromatic ring is slow on the NMR time scale. In the oxidized form, only two resonances are present, indicating that the chemical shifts of the four aromatic protons are pairwise averaged upon rotation. Four signals for the aromatic protons have been observed for the cyanide adduct of the Met80Ala mutant, where the OH group of Tyr67 is H-bonded to the cyanide moiety.

The structure of oxidized cyt *c* in the complex with CcP is particularly meaningful, as it indicates which of the

peripheral residues are involved in protein−protein interactions. In particular, Gln16, Asn70, Lys73, and Lys87 (which are involved in H bonds with CcP) and Leu9, Arg13, Ala81, Phe82, Gly83, and Lys86 (which are involved in hydrophobic interactions) are likely to be important in complex formation (Pelletier & Kraut, 1992). Many of these residues have the same conformation in the complex as they do in the solution structure of reduced cyt *c* (Baistrocchi et al., 1996) and, as our present work shows, in the solution structure of uncomplexed oxidized cyt *c* as well. However, there are some differences in the orientation of the Gln16 side chain in the various structures. In solution, this side chain has the same orientation as in the complex; i.e., it is oriented so that it can form an internal hydrogen bond with the carbonyl oxygen of Arg13, whereas in the crystal structures of uncomplexed cytochrome *c*, it is folded back to form a hydrogen bond with its own backbone amide nitrogen. Minor differences also are observed in the terminal region of the side chains of Lys73 and Lys87 (which are possible hydrogen bond donors to CcP) and Leu9 (which is one of the residues involved in hydrophobic interprotein interactions). In the present structure, the Lys86 side chain has a conformation similar to that in the solution structure of the reduced form, but slightly different from that found in the crystal structures of the complexed and uncomplexed protein. The side chain of Arg13, which is relatively well-defined in the present structure (rmsd value of 1.37 Å for the side chain), and which is thought to be involved in interactions with cytochrome b_5 (Salemme, 1976; Wendoloski et al., 1987; Northrup et al., 1993), differs in conformation from that in the solution structure of the reduced protein as well as from that in the three crystal structures.

Concluding Remarks. The present solution structure of oxidized cyt *c*, obtained without isotope labeling, has a relatively high resolution thanks to the use of the pseudocontact shifts together with NOE constraints, in both DG calculations and restained energy minimization.

The elements of secondary structure are the same as in the reduced species, which is a finding that is consistent with the corresponding X-ray structures. In this respect, the yeast protein solution structures differ from those of horse heart cyt *c*; in the case of the horse protein, dramatic changes between oxidized and reduced species have been reported (Qi et al., 1996).

The solution structures of *S. cerevisiae* cyt *c* show a change in the H bond between the amide proton of Gly41 and propionate 7, which is in accord with the X-ray structures. This bond could not be detected in the solution structure of horse cyt *c*, where the structure determination was reported to be poor around the paramagnetic center (Qi et al., 1996). It has been suggested that the Gly41−propionate 7 H bond is part of a direct tunneling pathway that is responsible for the relatively strong coupling between the heme and a Ru complex bonded to His39 in the protein (Winkler & Gray, 1992).

The flexibility appears to be larger in the oxidized protein than in the reduced one, as shown by the exchangeability of NHs in protein segments 14−26 and 75−82. This observation is also consistent with the decreased stability of the oxidized form. This conformational flexibility probably extends to several residues in the protein. In particular, the side chain of Tyr67 rotates rapidly in the oxidized form, while it has a rigid conformation in the reduced protein.

ACKNOWLEDGMENT

Experiments were performed with the instrumentation of the Florence Laboratory of Relaxometry and Magnetic Resonance on Paramagnetic Metalloproteins, Large Scale Facility of the European Union.

SUPPORTING INFORMATION AVAILABLE

Tables containing proton assignments (shift values measured at 303 K), experimental NOESY intensities, and hydrogen bond and pseudocontact shift constraints used for the structure calculations (19 pages). Ordering information is given on any current masthead page.

REFERENCES

Bai, Y. W., Sosnick, T. R., Mayne, L., & Englander, S. W. (1995) *Science 269*, 192−197.
Baistrocchi, P., Banci, L., Bertini, I., Turano, P., Bren, K. L., & Gray, H. B. (1996) *Biochemistry 35*, 13788−13796.
Banci, L., Bertini, I., Luchinat, C., Piccioli, M., Scozzafava, A., & Turano, P. (1989) *Inorg. Chem. 28*, 4650−4656.
Banci, L., Bertini, I., Bren, K. L., Gray, H. B., Sompornpisut, P., & Turano, P. (1995) *Biochemistry 34*, 11385−11398.
Banci, L., Bertini, I., Bren, K. L., Cremonini, M. A., Gray, H. B., Luchinat, C., & Turano, P. (1996a) *JBIC 1*, 117−126.
Banci, L., Bertini, I., Gori Savellini, G., Romagnoli, A., Turano, P., Cremonini, M. A., Luchinat, C., & Gray, H. B. (1996b) *Proteins* (in press).
Bax, A., & Freeman, R. (1981) *J. Magn. Reson. 44*, 542−561.
Bax, A., & Davis, D. G. (1985) *J. Magn. Reson. 65*, 355−360.
Bax, A., Freeman, R., & Morris, G. (1981) *J. Magn. Reson. 42*, 164−168.
Berghuis, A. M., & Brayer, G. D. (1992) *J. Mol. Biol. 223*, 959−976.
Berghuis, A. M., Guillemette, J. G., McLendon, G., Sherman, F., Smith, M., & Brayer, G. D. (1994) *J. Mol. Biol. 236*, 786−799.
Bertini, I., & Luchinat, C. (1986) *NMR of paramagnetic molecules in biological systems*, Benjamin/Cummings, Menlo Park, CA.
Bertini, I., & Turano, P. (1994) in *NMR of paramagnetic macromolecules. NATO ASI Series* (La Mar, G. N., Ed.) Kluwer Academic, Dordrecht.
Bertini, I., & Luchinat, C. (1996) NMR of paramagnetic substances, *Coord. Chem. Rev. 150*, 1−300.
Bixler, J., Bakker, G., & McLendon, G. (1992) *J. Am. Chem. Soc. 114*, 6938.
Blackledge, M. J., Medvedeva, S., Poncin, M., Guerlesquin, F., Bruschi, M., & Marion, D. (1995) *J. Mol. Biol. 245*, 661−681.
Blanchard, L., Blackledge, M. J., Marion, D., & Guerlesquin, F. (1996) *FEBS Lett. 388*, 203−209.
Casimiro, D. R., Richards, J. H., Winkler, J. R., & Gray, H. B. (1993) *J. Phys. Chem. 97*, 13073−13077.
Cohen, D. S., & Pielak, G. J. (1995) *J. Am. Chem. Soc. 117*, 1675−1677.
Detlefsen, D. J., Thanabal, V., Pecoraro, V. L., & Wagner, G. (1991) *Biochemistry 30*, 9040−9046.
Doyle, D. F., Parikh, S., Alcazar-Roman, L., Cole, J. L., & Pielak, G. J. (1996) *Biochemistry 35*, 7403−7411.
Eccles, C., Güntert, P., Billeter, M., & Wüthrich, K. (1991) *J. Biomol. NMR 1*, 111−130.
Elove, G. A., Bhuyan, A. K., & Roder, H. (1994) *Biochemistry 33*, 6925−6935.
Englander, S. W. (1992) *Science 256*, 1684.
Englander, S. W., & Kallenbach, N. R. (1983) *Q. Rev. Biophys. 16*, 521−655.
Feng, Y. Q., Roder, H., & Englander, S. W. (1990) *Biochemistry 29*, 3494−3504.
Gao, Y., Boyd, J., Williams, R. J. P., & Pielak, G. J. (1990) *Biochemistry 29*, 6994−7003.
Gao, Y., Boyd, J., Pielak, G. J., & Williams, R. J. P. (1991a) *Biochemistry 30*, 1928−1934.
Gao, Y., Boyd, J., Pielak, G. J., & Williams, R. J. P. (1991b) *Biochemistry 30*, 7033−7040.

Gochin, M., & Roder, H. (1995) *Protein Sci. 4*, 296−305.
Gray, H. B., & Winkler, J. R. (1996) *Annu. Rev. Biochem. 65*, 537−561.
Güntert, P., & Wüthrich, K. (1991) *J. Biomol. NMR 1*, 447−456.
Güntert, P., Braun, W., & Wüthrich, K. (1991) *J. Mol. Biol. 217*, 517−530.
Hilgen-Willis, S., Bowden, E. F., & Pielak, G. J. (1993) *J. Inorg. Biochem. 51*, 649−653.
Hvidt, A., & Nielsen, S. O. (1966) *Adv. Protein Chem. 21*, 287.
Inubushi, T., & Becker, E. D. (1983) *J. Magn. Reson. 51*, 128−133.
Kraulis, P. J. (1991) *J. Appl. Crystallogr. 24*, 946−950.
La Mar, G. N., Horrocks, W. D. W., & Holm, R. H., Eds. (1973) *NMR of Paramagnetic Molecules*, Academic Press, New York.
Langen, R., Colon, J. L., Casimiro, D. R., Karpishin, J. R., Winkler, J. R., & Gray, H. B. (1996) *JBIC 1*, 221−225.
Lefevre, J.-F., & Jardetzky, O. (1994) *FEBS Lett. 338*, 246−250.
Louie, G. V., & Brayer, G. D. (1990) *J. Mol. Biol. 214*, 527−555.
Lu, Y., Casimiro, D. R., Bren, K. L., Richards, J. H., & Gray, H. B. (1993) *Proc. Natl. Acad. Sci. U.S.A. 90*, 11456−11459.
Macura, S., Wüthrich, K., & Ernst, R. R. (1982) *J. Magn. Reson. 47*, 351−357.
Marion, D., & Guerlesquin, F. (1992) *Biochemistry 31*, 8171−8179.
Marion, D., & Wüthrich, K. (1983) *Biochem. Biophys. Res. Commun. 113*, 967−974.
Marmorino, J. L., Auld, D. S., Betz, D. S., Doyle, D. F., Young, G. B., & Pielak, G. J. (1993) *Protein Sci. 2*, 1966−1974.
Mer, G., Kellenberg, C., Koehl, P., Stote, R., Sorokine, O., van Dorsselaer, A., Luu, B., Hietter, H., & Lefevre, J.-F. (1994) *Biochemistry 33*, 15397−15407.
Mines, G. A., Pascher, T., Lee, S. C., Winkler, J. R., & Gray, H. B. (1996) *Chem. Biol. 3*, 491−497.
Northrup, S. H., Thomasson, K. A., Miller, C. M., Barker, P. D., Eltis, L. D., Guillemette, J. G., Inglis, S. C., & Mauk, A. G. (1993) *Biochemistry 32*, 6613−6623.
Pascher, T., Chesick, J. P., Winkler, J. R., & Gray, H. B. (1996) *Science 271*, 1558−1560.
Pearlman, D. A., & Case, D. A. (1991) *SANDER*, University of California, San Francisco.
Pelletier, H., & Kraut, J. (1992) *Science 258*, 1748−1755.
Piotto, M., Saudek, V., & Sklenar, V. (1992) *J. Biomol. NMR 2*, 661−666.
Qi, P. X., Beckman, R. A., & Wand, A. J. (1996) *Biochemistry 35*, 12275−12286.
Salemme, F. R. (1976) *J. Mol. Biol. 102*, 563−568.
Scott, R. A. (1996) in *Cytochrome c. A multidisciplinary approach* (Scott, R. A., & Mauk, A. G., Eds.) pp 515−541, University Science Books, Sausalito, CA.
Sklenar, V., Piotto, M., Leppik, R., & Saudek, V. (1993) *J. Magn. Reson., Ser. A 102*, 241−245.
Takano, T., & Dickerson, R. E. (1981a) *J. Mol. Biol. 153*, 79−94.
Takano, T., & Dickerson, R. E. (1981b) *J. Mol. Biol. 153*, 95−155.
Turner, D. L. (1995) *Eur. J. Biochem. 227*, 829−837.
Wagner, G., Hyberts, S., & Peng, J. W. (1993) in *NMR of Proteins*, pp 220−257, Macmillan Press, New York.
Wendoloski, J. J., Matthew, J. B., Weber, P. C., & Salemme, F. R. (1987) *Science 238*, 794−797.
Williams, G., Clayden, N. J., Moore, G. R., & Williams, R. J. P. (1985) *J. Mol. Biol. 183*, 447−460.
Winkler, J. R., & Gray, H. B. (1992) *Chem. Rev. 92*, 369−379.
Wüthrich, K. (1986) *NMR of Proteins and Nucleic Acids*, Wiley, New York.

BI963025C